Apr 27th, 2021 - 1:30 PM

Thermal modeling of li-ion batteries using SP+3D model

Derrick Barger

Modeling of Thermal and Electrochemical Behavior of Lithium-Ion Batteries Using a Single Particle Model with Coupled 3D Heat Generation

Researcher: Derrick Barger

Faculty Advisors: Dr. Jonghyun Park and Dr. Robert Landers

Missouri University of Science and Technology department of mechanical and aerospace engineering

Abstract

An ideal battery model must gather sufficient electrochemical data about the system while remaining computationally efficient. To prevent failure from thermal runaway, understanding the thermal characteristics of a battery is essential.

To achieve this, we have developed a single particle (SP) model, a simplified but accurate approach to battery modeling, and compared this to a previously designed 3D model. After validating the battery electrochemistry, equations were introduced to calculate the heat generation with a coupled 3D heat transfer component to provide data on the cell temperature. This same model was used to simulate a multi-cell pack.

The results indicate close electrochemical and thermal accuracy between the two models at multiple discharge rates. However, the SP+3D model can reach these results more than 60 times faster than the 3D model. By more efficiently simulating the battery discharge, the SP+3D model can be applied to a variety of future test scenarios.

Introduction

As humanity's reliance on sustainable fuel sources grows, as does our need for more advanced energy storage systems. Producing and testing on physical batteries can be a time consuming and costly process, so it is necessary to have methods to virtually simulate and model new battery technology. Furthermore, because batteries can be quite complex and difficult to observe during operation, battery models are needed to provide real time data on a battery system. This is called a battery management system (BMS) and they provide important data on a battery's health.

There are a variety of ways to simulate a battery, and there is typically a trade off between amount of data and computation time. The standard 3D modeling method provides the most accurate overview of a battery at the cost of a very lengthy computation time. This makes it more difficult to use for research and entirely impractical for real world application. In contrast, the single particle model sacrifices increased electrochemical data for computation time. The SP model is unique in that it assumes both the anode and cathode are spherical particles of identical size and shape. This assumption greatly simplifies the amount of computational power required to perform the model by reducing the amount of partial differential equations needed. Despite the simplifications of the battery system, the SP model retains a high degree of accuracy relative to other more complex modeling methods, though its lack of electrolyte physics causes the model to break down at high C rates. This simplification is necessary for the model to be implemented to a BMS because traditional 3D models are far too computationally demanding to practically provide real time data.

One of the most dangerous failures a battery can experience is called thermal runaway. This catastrophic failure occurs when the cell temperature becomes too high, which can cause a chain reaction to occur that leads to combustion. Therefore, understanding the thermal behavior of a battery is incredibly important. The goal of this research project is to define a battery model that can accurately describe the battery electrochemistry and thermal behavior across a 3D space. This is achieved by coupling a single particle model with a 3D heat transfer component. Current models either lack the ability to define heat rates on a 3D space or take too long to compute to be used in a real-world system.

Single Particle Model Design and Governing Equations

By assuming both electrodes are perfect, spherical particles with a uniform current distribution along their thickness, the concentration of lithium ions in the electrodes can be solved for using Fick's second law of diffusion with respect to the particle radius. This is shown in the equation

$$\frac{\partial c_{s,j}}{\partial t} = \frac{D_{s,j}}{r^2}\frac{\partial}{\partial r}\left(r^2\frac{\partial c_{s,j}}{\partial r}\right) \quad (1)\ [2]$$

where c_s is the concentration, D_s is the diffusion coefficient of the particle, and r is the radius, and t is time. We can assume that ion concentration in the center of the particle is zero from symmetry. Thus the boundary conditions of equation (1) can be described as:

$$\left(D_{sj}\frac{\partial c_{sj}}{\partial r}\right)_{r=0} = 0 \quad (2)\ [2]$$

$$\left(D_{sj}\frac{\partial c_{sj}}{\partial r}\right)_{r=R_j} = -J_j \quad (3)\ [2]$$

where r=0 is the center of the particle, R_j is the surface of the particle, and J_j is the molar flux of lithium ions at the surface, and j refers to positive/negative (cathode/anode).

The concentration found with equation (3) be used to determine the SOC (current Li-ion concentration divided by the maximum Li-ion concentration). This relationship is demonstrated by:

$$x_j = \frac{c_{s,j}}{c_{s,j,max}} \quad (4)\ [2]$$

This equation can be used to derive the initial and surface SOC by using the appropriate values for ion concentration. The equations for the initial and surface SOC are shown with the equations

$$x_{ini,j} = \frac{c_{s,ini,j}}{c_{s,j,max}} \quad (5)\ [2]$$

$$x_{j,surf} = \frac{c_{s,j}|_{r=R_j}}{c_{s,j,max}} \quad (6)\ [2]$$

Using the calculatable SOC and breakdown of the electrochemical lithium-ion reactions in the previous section allows the calculation of the rate of the reaction. This is expressed with the Butler-Volmer equation.

$$J_j = k_j c_{s,j,max} c_e^{0.5}\left(1-x_{j,surf}\right)^{0.5} x_{j,surf}^{0.5}\left[\exp\left(\frac{.5F}{RT}\eta_j\right) - \exp\left(-\frac{0.5F}{RT}\eta_j\right)\right] \quad (7)\ [2]$$

where k_j is the temperature-dependent reaction rate constant, R is the universal gas constant, T is temperature, and F is Faraday's constant. The electrolyte concentration in solution phase c_e is assumed to be constant in the SP model. The overpotential η_j is defined as

$$\eta_j = \phi_{1,j} - \phi_{2,j} - U_j \quad (8)\ [2]$$

where $\phi_{1,j}$ is the solid phase potential, $\phi_{2,j}$ is the solution phase potential, and U_j is the open circuit potential that depends on the surface SOC and temperature. The OCP is generally a function of the normalized surface concentration, $c_{s,j,surf}(t)/c_{s,j,max}(t)$, and temperature. Because of this, the potential difference can be obtained from the equation (10).

$$\eta_j(t) = \frac{2RT}{F}\ln\left[m_j(t) + \sqrt{m_j^2(t)+1}\right] \quad (9)\ [1]$$

$$\text{where } mj(t) = \frac{J_j}{2k_j c_{s,j,max} c_e^{0.5} \left(1 - x_{j,surf}\right)^{0.5} x_{j,surf}^{0.5}}$$

(j=p/n)

The voltage of a cell is modeled by calculating the solid phase potential difference between the positive and negative ends of the cell.

$$V_{cell}(t) = \phi_{1,p}(t)|_{x=L} - \phi_{1,n}(t)|_{x=0}$$

$$= (\eta_p + \phi_{2,p}(t)|_{x=L} + U_p) - (\eta_n + \phi_{2,n}(t)|_{x=0} + U_n)$$

$$= \left(\frac{2RT}{F} \ln\left[m_p(t) + \sqrt{m_p^2(t) + 1}\right] + \phi_{2,p}(t)|_{x=L} + x_{p,surf} U_p\right)$$

$$- \left(\frac{2RT}{F} \ln\left[m_n(t) + \sqrt{m_n^2(t) + 1}\right] + \phi_{2,n}(t)|_{x=0} + x_{n,surf} U_n\right) \quad (10)\ [1]$$

Thermal Model Coupling

In order to decrease computation time, a 3D thermal model was coupled with the SP model presented above to simulate heat generation. This variable temperature causes changes to the internal workings of the battery.

Alterations to solid phase lithium diffusivity: The standard SP model assumes a constant rate of lithium diffusion at the positive and negative electrodes because the internal and ambient temperature of the battery was held constant. Increasing the temperature increases the kinetic energy that molecules possess; therefore, the rate of diffusion will increase as the temperature increases. This is also one of the reasons that batteries perform more poorly at very low temperatures (low temperature causes decreased diffusion). This temperature dependent relationship is shown through the equation:

$$D_{s,j}(t) = D_{s,j,ref} * e^{\frac{E_{a,d,j}}{R}\left(\frac{1}{T} - \frac{1}{T_{ref}}\right)} \quad (11)\ [2]$$

Where $D_{s,j}$ is the solid phase lithium diffusion, $D_{s,j,ref}$ is the solid phase lithium diffusion at T_{ref}, $E_{a,d,j}$ is the activation energy at the electrode, R is the universal gas constant, T is the current battery temperature, and T_{ref} is the starting cell temperature, and j is either the positive or negative electrode.

Alterations to reaction rate coefficients: The rate of a reaction is also highly dependent on temperature. Increasing the temperature increases reaction rates because of the disproportionately large increase in the number of high energy collisions. It is only these collisions (possessing at least the activation energy for the reaction) which result in a reaction. Thus, following the same rationale as with diffusion, at low temperatures, the amount of high energy collisions will decrease from the molecules being less excited. This reaction rate-temperature relationship is demonstrated below:

$$k_j(t) = k_{j,ref} * e^{\frac{E_{a,r,j}}{R}\left(\frac{1}{T} - \frac{1}{T_{ref}}\right)} \quad (12)\ [2]$$

Where k_j is the reaction rate coefficient at changing temperature, $k_{j,ref}$ is the reaction rate coefficient at T_{ref}, and $E_{a,r,j}$ is the activation energy for the reaction rate constant.

Heat generation equations: Thermodynamic expressions for irreversible, reversible, and total heat generation are needed to simulate the heat generation of a battery cell. The irreversible heat generation is largely dependent on the cell's internal resistance; therefore, irreversible heat generation is much higher when the cell is discharging at a high C rate. Irreversible heat generation should always be positive

regardless of the reaction direction. Irreversible heat generation can be described mathematically with the equation:

$$Q_{irr} = I(\eta_p - \eta_n + IR_{cell}) \quad (13)\ [2]$$

Where I is the applied current, η_p is the positive overpotential, η_n is the negative overpotential, and R_{cell} is the total cell resistance.

The reversible heat is caused by the reaction entropy change mainly caused by the lithium ion insertion/extraction between cathode and anode, which is determined by the entropic coefficients of the electrodes, which are related to open-circuit voltage at different temperatures. The reversible heat generated can either be positive or negative based on the reaction direction. This makes the reversible heat generation much more prominent under lower C rates. Reversible heat gain in the cell is calculated as:

$$Q_{rev} = IT\left[\frac{\partial U_p}{\partial T} - \frac{\partial U_n}{\partial T}\right] \quad (14)\ [2]$$

Where Q_{rev} is the reversible heat generation, $\frac{\partial U_p}{\partial T}$ is entropy coefficient profile for the cathode, and $\frac{\partial U_n}{\partial T}$ is the entropy coefficient profile for the anode. The values for $\frac{\partial U_j}{\partial T}$ can be quite challenging to determine, so my results will use a predetermined value from (Guo, Sikha, & White, 2011b). The value of reversible heat generation is heavily dependent on the material used in the electrodes and must be recalculated for different materials used. For the electrode materials $LiCoO_2$ and MCMB, the entropy coefficient profiles can be shown using the two equations respectively:

$$\frac{\partial U_p}{\partial T} = \frac{-0.19952+0.92837x_p-1.36455x_p^2+0.61154x_p^3}{1-5.66148x_p+11.47636x_p^2-9.82431x_p^3+4.04876x_p^4} \quad (15)\ [2]$$

$$\frac{\partial U_n}{\partial T} = \frac{0.00547 + 3.2993x_n - 91.7932x_n^2 + 1004.911x_n^3 - 5812.2781x_n^4 + 19{,}329.7549x_n^5 - 37{,}147.8947x_n^6 + 38{,}379.1813x_n^7 - 16{,}515.0531x_n^8}{1 - 48.0929x_n + 1017.2348x_n^2 - 10{,}481.8042x_n^3 + 59{,}431.3x_n^4 - 195{,}881.649x_n^5 + 374{,}577.315x_n^6 - 385{,}821.161x_n^7 + 165{,}705.8597x_n^8}$$

(16) [2]

The total heat gain of the battery can be represented by the addition of its two components, yielding:

$$Q_{tot} = Q_{rev} + Q_{irr} \quad (17)[2]$$

Heat Transfer Component: A 3D heat transfer in solids component was coupled with the original SP model. COMSOL provides some of the initial equations necessary to model the heat generation. The primary equation used to calculate the heat transfer is:

$$\rho C_p \frac{\partial T}{\partial t} + \rho C_p u * \nabla T + \nabla \cdot (q + q_r) = Q + Q_{ted} \quad (18)[2]$$

Where ρ is the material density (kg/m^3), C_p is the material specific heat (J/(kg*K)), $\frac{\partial T}{\partial t}$ is the partial derivative of temperature with respect to time, u is the velocity vector of translational motion (m/s), q is the heat flux by conduction (W/m^2), q_r is the heat flux by radiation (W/m^2), Q_{ted} is the thermoelastic damping, and Q contains the additional heat sources (W/m^3). The presented simulation does not have values for all of these parameters (such as for u), but they are included automatically by COMSOL and ignored if unneeded for calculations.

Next, the model allows input for the material thermal conductivity (k), material density, and material specific heat.

Boundaries were established at each cell surface to calculate the thermal heat flux using a COMSOL programed function.

Lastly, a heat source was established in the 3D space. This was defined by:

$$Q_0 = P_0/V \tag{19}[2]$$

Where Q_0 is the heat source, P_0 is the heat rate, and V is the volume enclosed by the specified domain.

Boundary conditions: A realistic battery simulation should consider how the surroundings also impact the battery temperature. This is especially relevant when the outside temperature is different than the battery's starting temperature. Modeling the heat flux through the battery's surface is represented with the equation:

$$q_0 = h(T_{ext} - T) \tag{20}[2]$$

Where q_0 is the rate of heat transfer between the cell and its surroundings, h is the heat transfer coefficient, T_{ext} is the external temperature, and T is the temperature of the cell.

This boundary condition is applied to the entire surface area of the cell. The impact from the heat flux has the greatest impact on the cell when there is a large temperature difference between the cell and its surrounding environment. The addition of this heat transfer boundary condition satisfies the general energy balance of the system which is demonstrated with the equation:

$$\rho v C_p \frac{dT}{dt} = Q_{tot} - q_0 \tag{21}[2]$$

Where ρ is the density, v is the volume, C_p is the specific heat, $\frac{dT}{dt}$ is the derivative of cell temperature with respect to time, and Q_{tot} is the total heat generation in the battery. Thus, the heat transfer conditions have a very significant impact on the cell's thermal behavior.

Adding thermal component to previous 3D model

Different battery models have their own strengths and weaknesses. To validate the new SP3D model proposed in this paper, it is necessary to compare it to a previously validated model. Electrochemical models, especially the 3D, are based on the theories of porous electrodes and concentrated solutions. In contrast to the SP model, the 3D model can capture the electrochemical reaction dynamics and predict the batteries' behavior under all operating conditions with increased accuracy. However, the model is much more difficult to simulate (in terms of structure and computation time) due to its complex coupling with numerous nonlinear partial differential equations, which restricts its application. This makes it so real time simulation of a battery cannot be accomplished with this model.

Understanding the cell temperature is imperative for many studies using the 3D method. While the heat generation formula is known, it must first be applied to a modeling program to be solved. The heat generation rate includes heat effect due to the electrode reaction, joule heating, and entropy change of the electrode reaction, which is expressed by

$$q_{P2D} = J\left(\Phi_s - \Phi_e - U_j + T\frac{\partial U_j}{\partial \mathrm{T}}\right) + \sigma_s^{eff}\nabla\Phi_s * \nabla\Phi_s + (\kappa_e^{eff}\nabla\Phi_e \cdot \nabla\Phi_e + \kappa_e^D \nabla \ln c_e * \nabla\Phi_e) \tag{22}[1]$$

Where Φ represents electric potential, s is the solid phase, e is the electrolyte, U_j is the open circuit potential that depends on the surface SOC and temperature, σ is the electronic conductivity of the

solid matrix, κ is the ionic conductivity of the electrolyte, and c_e is the salt concentration in the electrolyte.

The three terms of this heat generation equation are the heat sources due to charge transfer at the electrode/electrolyte interfaces and the entropy change and from the joule heating in the solid active and electrolyte phases, respectively. For the joule heating in the solution phase, the second half can be negated because the diffusional properties have a negligible effect on heat generation

A working 3D simulation for an NMC battery was altered to work for an LMO battery.

The 3D cell being simulated is broken up into separate geometries for cathode, anode, and separator. There is convective heat transfer between the cell and the ambient environment at all outside surface boundaries. It should be noted that the heat rate (q) for the cathode and anode is different.

Material Properties and Test conditions

The following tests are simulated using COMSOL and depict a lithium-ion battery composed of a graphite anode (Li_xC_6) and a $Li_yMn_2O_4$ cathode. This model defines end-of discharge as the time cell potential reaches 3V. This is determined by the standard workable voltage range of an LMO battery. All simulations were tested at 1C (a current density corresponding to a theoretical full discharge in one hour) and this was found to equal approximately 15 A/m^2. Further tests were conducted at 2C and 5C. The battery is in an ambient temperature of 298.15K and experiences only convective heat flux in stagnant air, therefore, the heat transfer coefficient is set to .1 (W/m^2K), unless otherwise specified. The battery has a specific heat capacity of 837.4 J/kgK, a thermal conductivity of 32.2 W/m^2K, and a density of 2007.7 kg/m^3. The 3D model and SP+3D model use identical starting concentrations, dimensions, and boundary conditions.

Results and Analysis for 1 Cell

First the two models were discharged at 1C, with heat generation terms for each model being plotted independently. This process was then repeated at 2C and 5C to gain a more thorough insight into the battery's performance under different discharge rates.

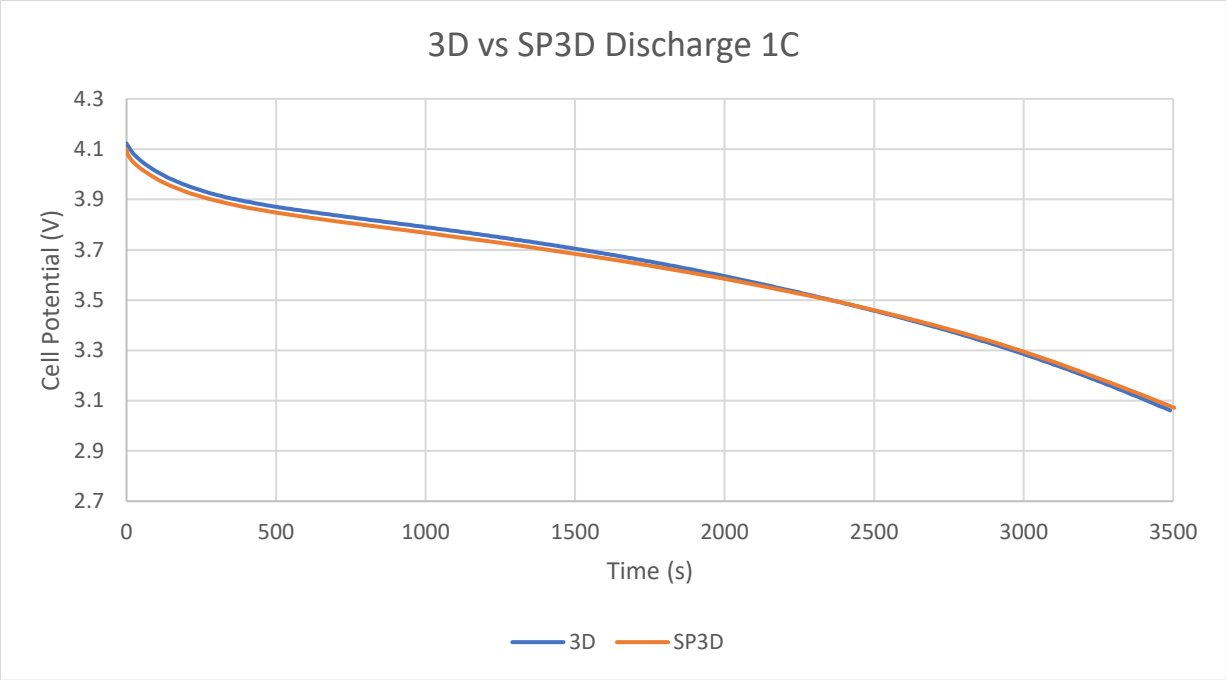

Figure 1: 3D vs SP3D 1C Discharge

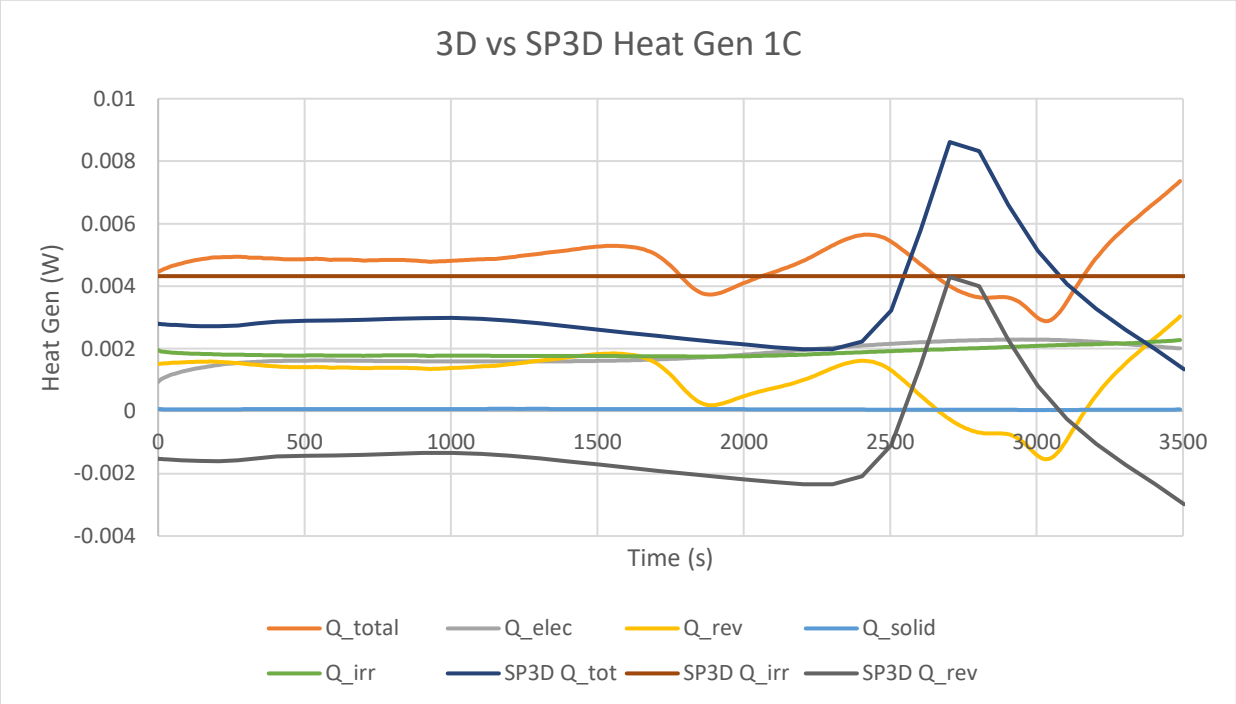

Figure 2: 3D vs SP3D 1C Heat Gen

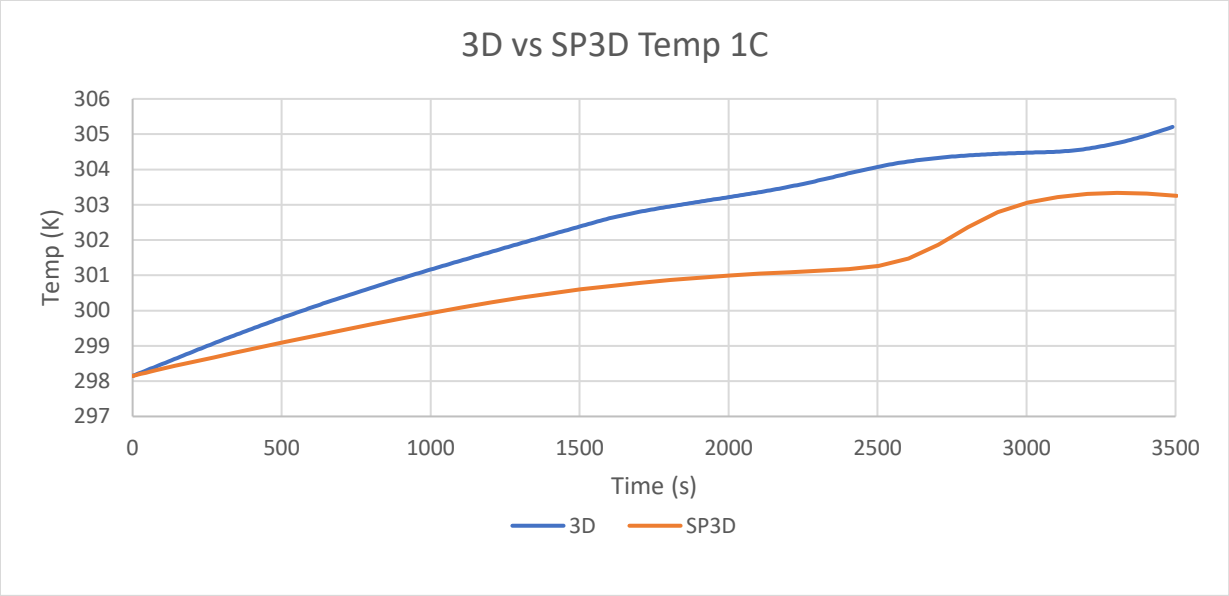

Figure 3: 3D vs SP3D 1C Cell Temp

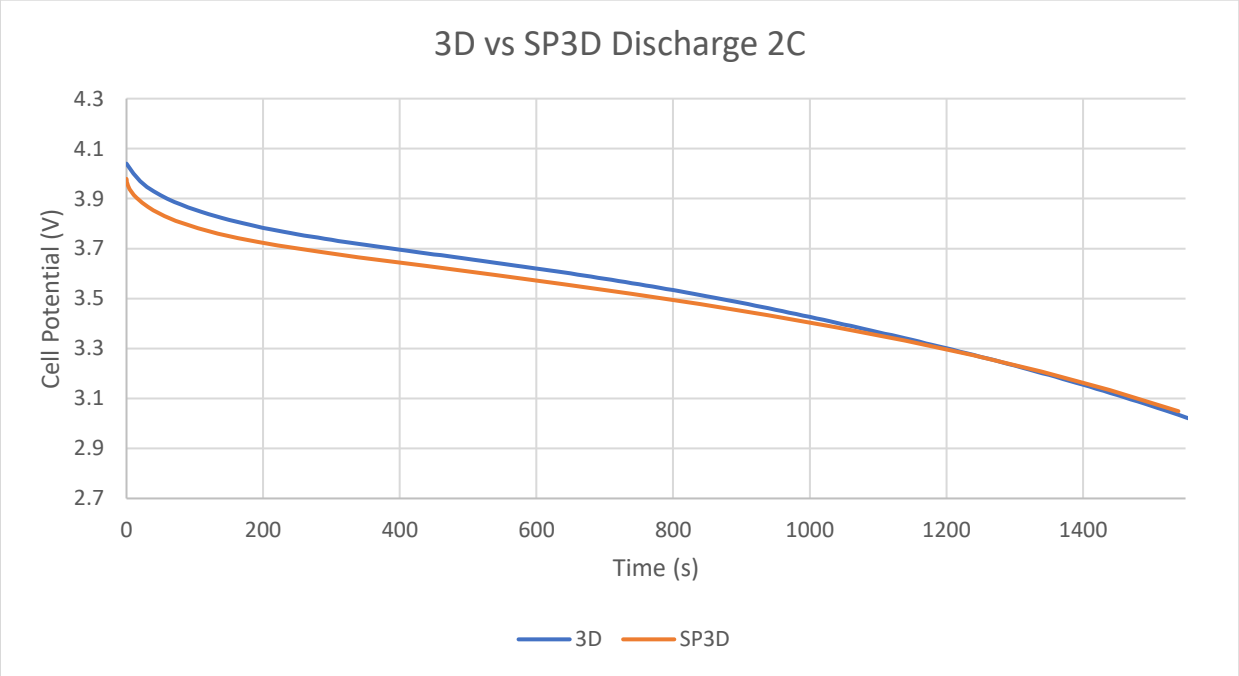

Figure 4: 3D vs SP3D 2C Discharge

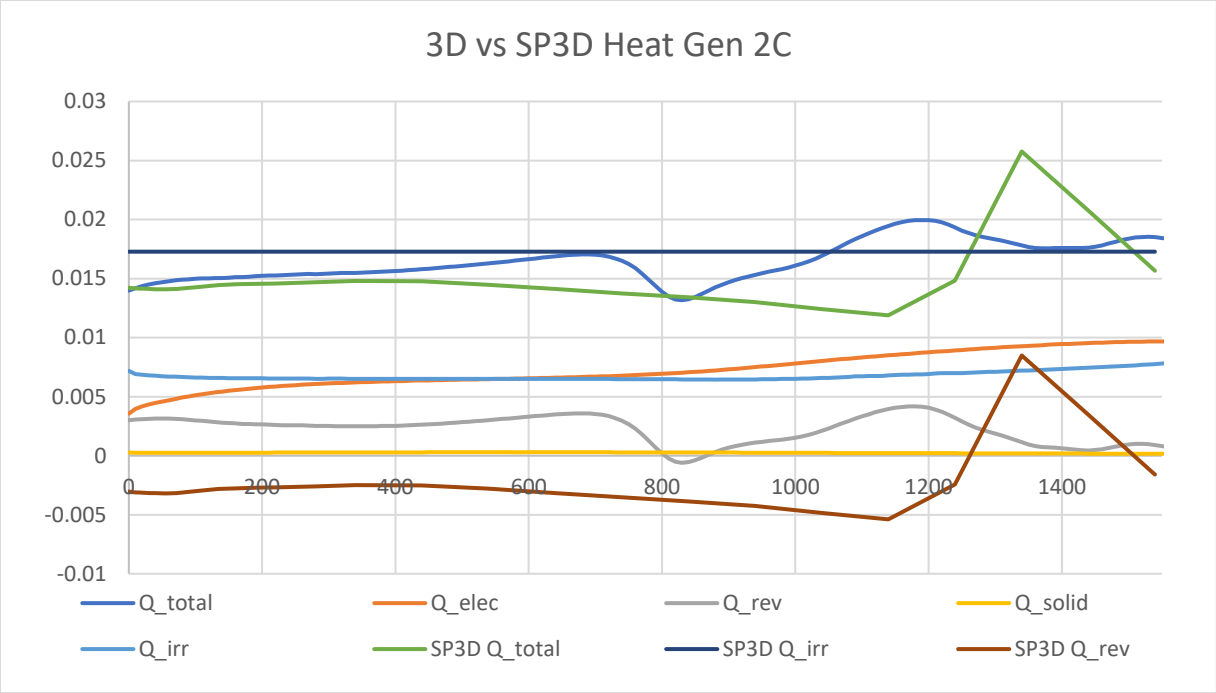

Figure 5: 3D vs SP3D 2C Heat Gen

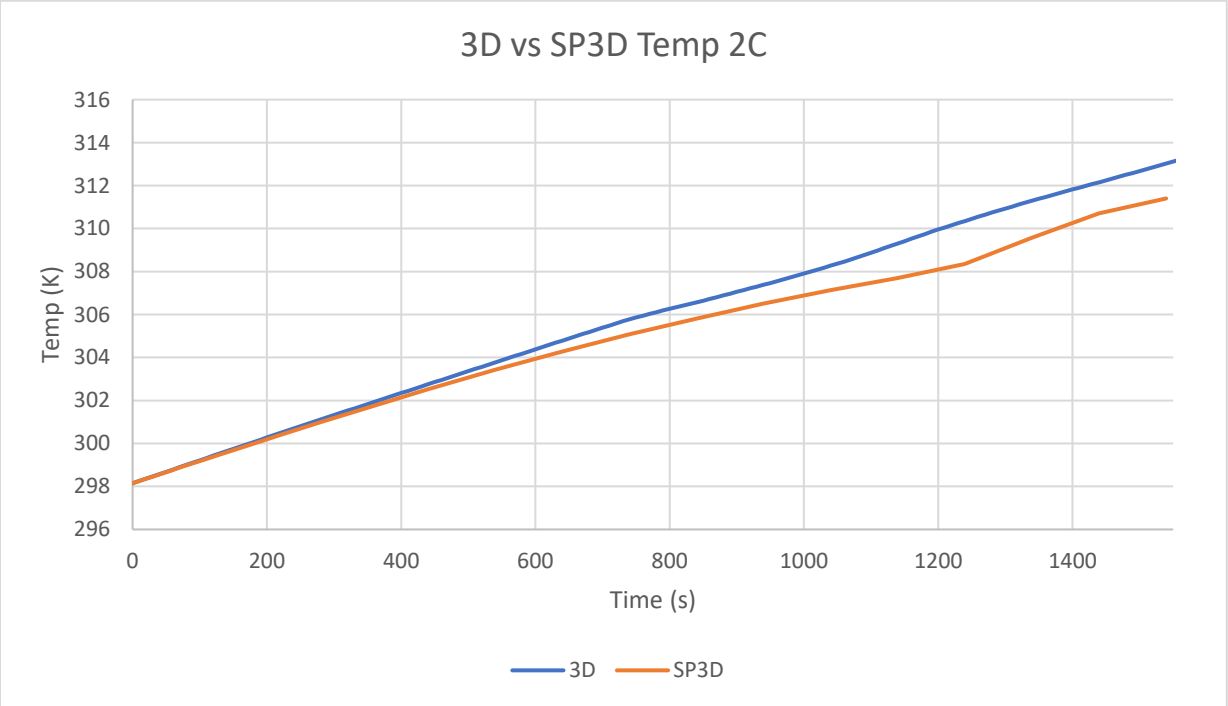

Figure 6: 3D vs SP3D 2C Cell Temp

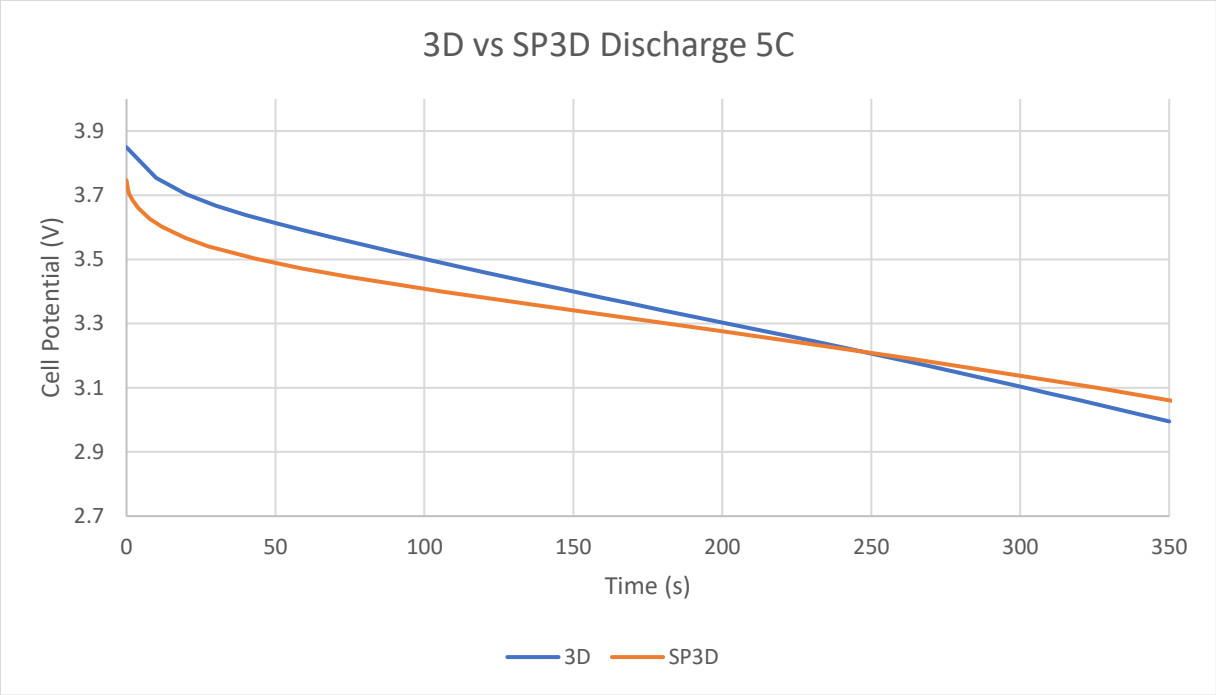

Figure 7: 3D vs SP3D 5C Discharge

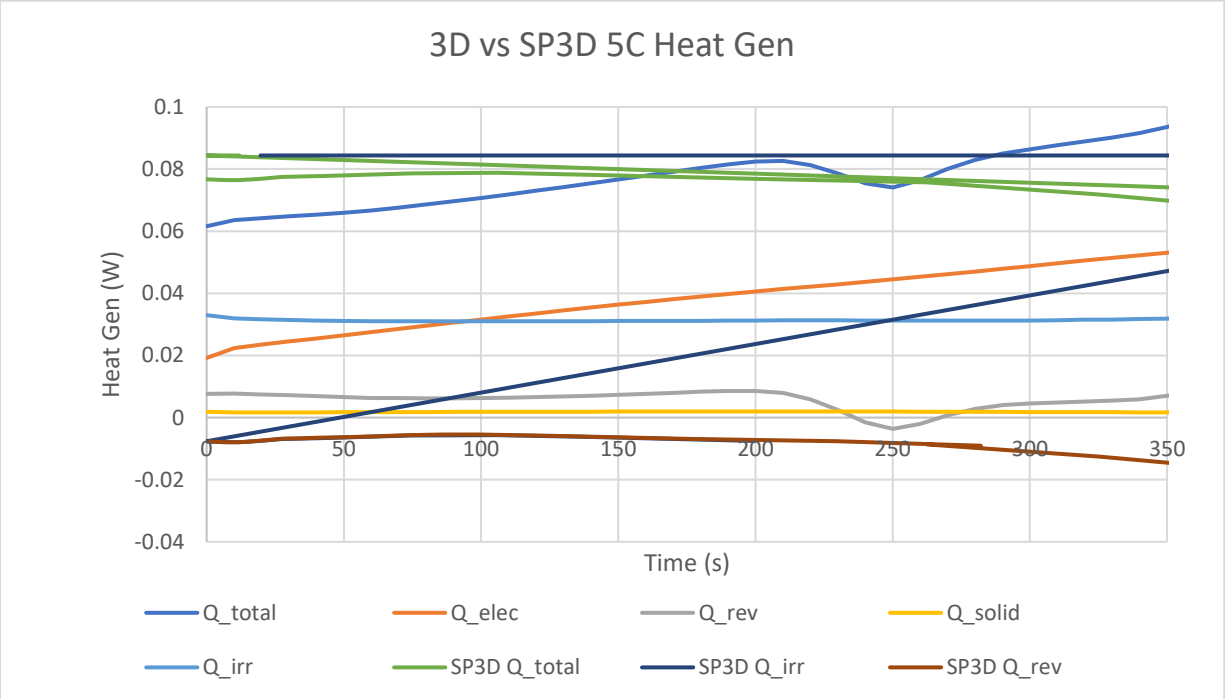

Figure 8: 3D vs SP3D 5C Heat Gen

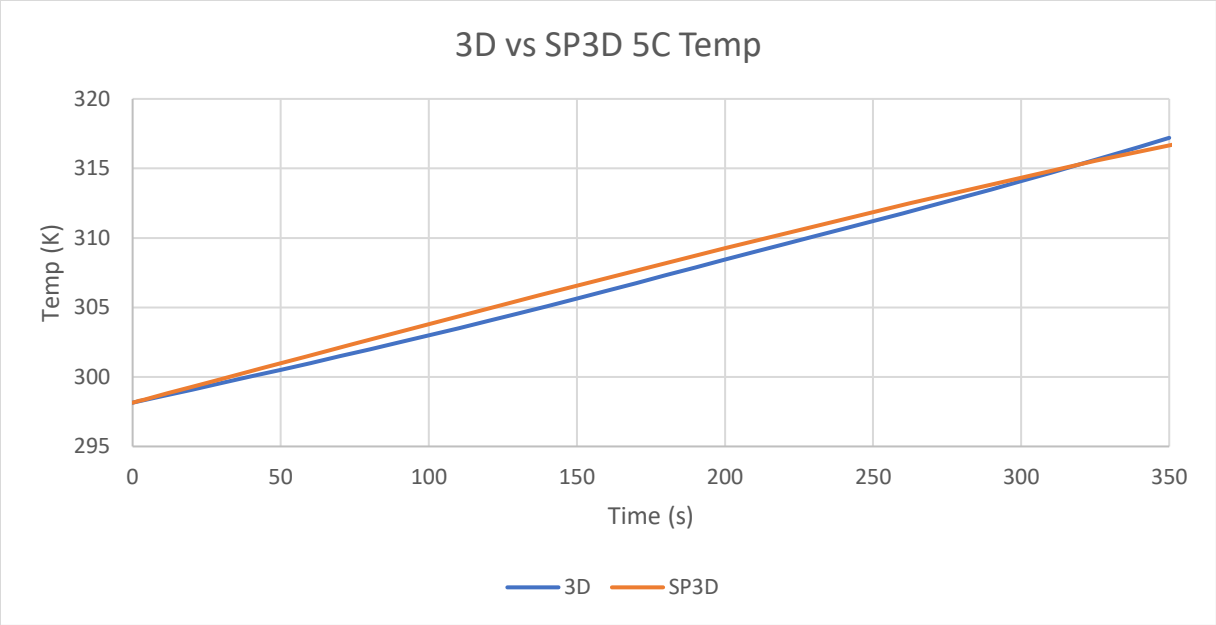

Figure 9: 3D vs SP3D 5C Cell Temp

The simplified state of the single particle model places a much stronger focus on the reversible heat generation when discharging at lower C rates than the 3D model. This is caused by the 3D model having more information on electrolyte concentrations than the SP model. However, SP3D has an increased reliance on the irreversible heat generation when the C rate increases. This can be explained by the heat generation terms for the battery including a squared applied current value. Therefore, one would expect the heat generation and cell temperature terms to be more similar between models as the C rate increases.

After running a variety of different tests, these results were found. The final cell temperature becomes increasingly similar as the C rate increases and the main difference in models (reversible heat generation) becomes less relevant. However, the discharge profile becomes increasingly dissimilar with higher C rates. The results are similar enough and just shows how the different models preform differently at different discharge rates.

Based on the similarity of results for the two models at 3 different C rates and the data following the theoretical and expected trend, it can be concluded that these models are accurately modeling the same thing off of their given inputs and parameters.

Results and Analysis for 2 Cell Pack Model

Batteries are typically used in battery packs, so it is important that a model can still provide an accurate picture of the battery when they are grouped together. To test this, the 3D and SP3D models were tested in a 2-cell serial connection. Ideally, this test would be conducted on a larger pack model, but the computation time for the 3D model is too lengthy for anything larger than a 2-cell model. The heat generation terms were not necessary to analyze in this test, so only discharge (electrochemistry) and cell temperature (heat flux) are graphed. These results are then compared to their single cell counterpart.

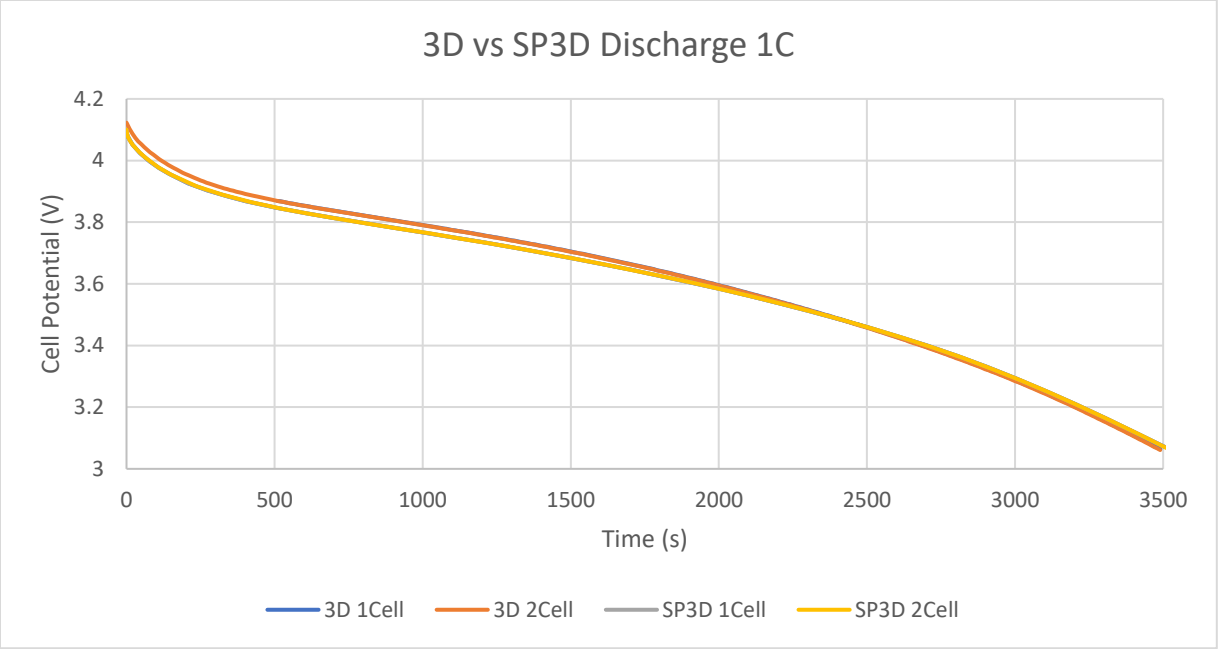

Figure 10: 3D vs SP3D 2Cell 1C Discharge

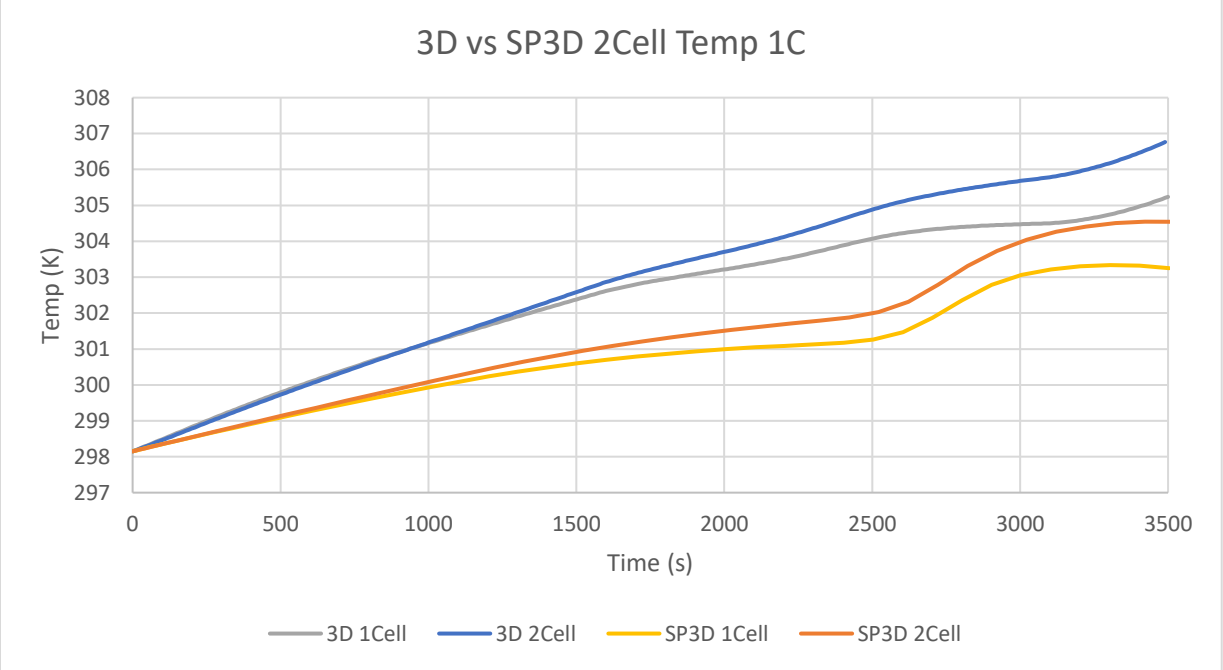

Figure 11: 3D vs SP3D 2Cell 1C Discharge

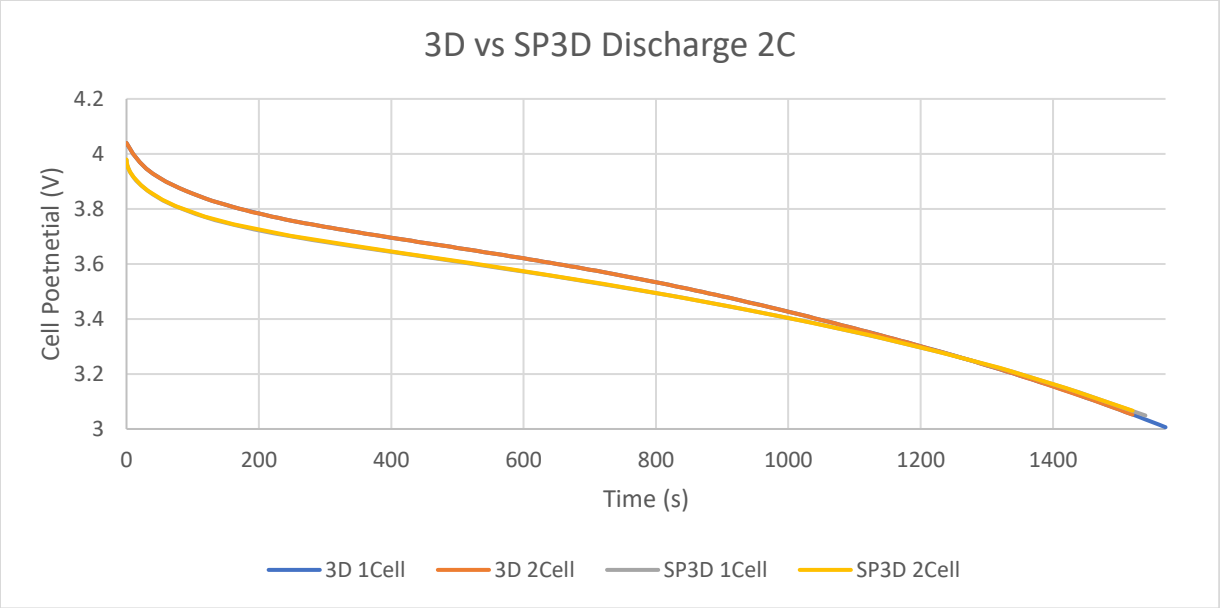

Figure 12: 3D vs SP3D 2Cell 2C Discharge

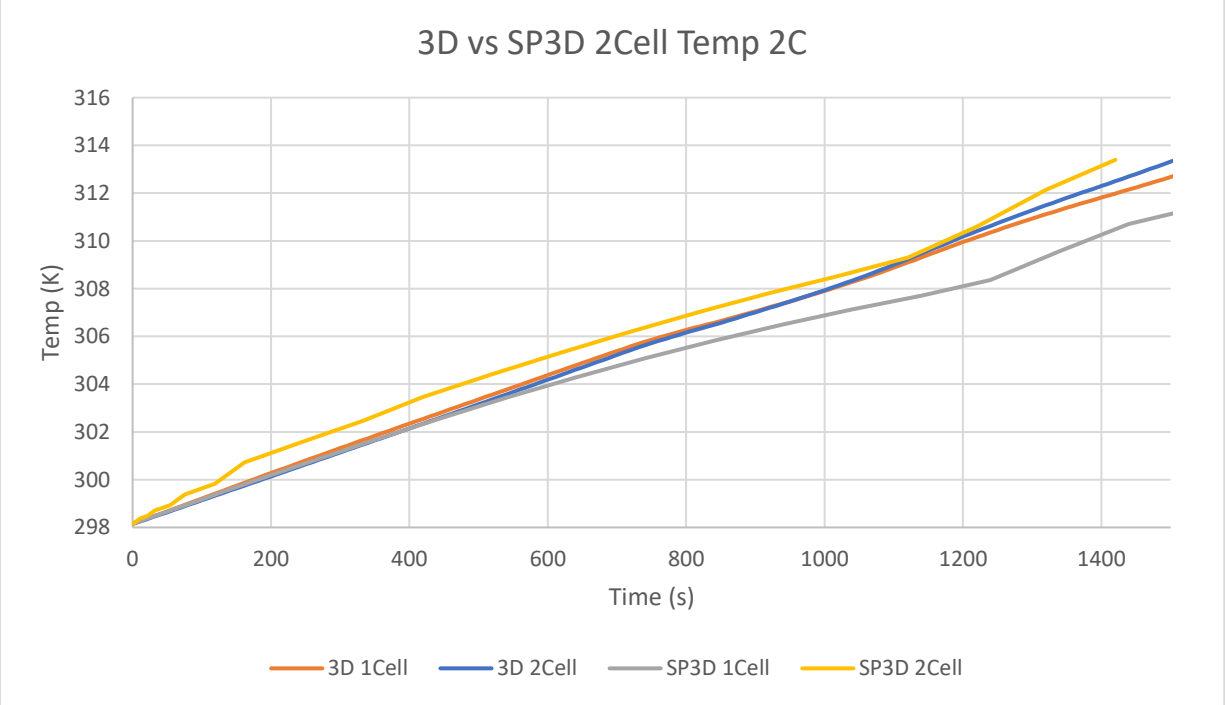

Figure 13: 3D vs SP3D 2Cell 2C Discharge

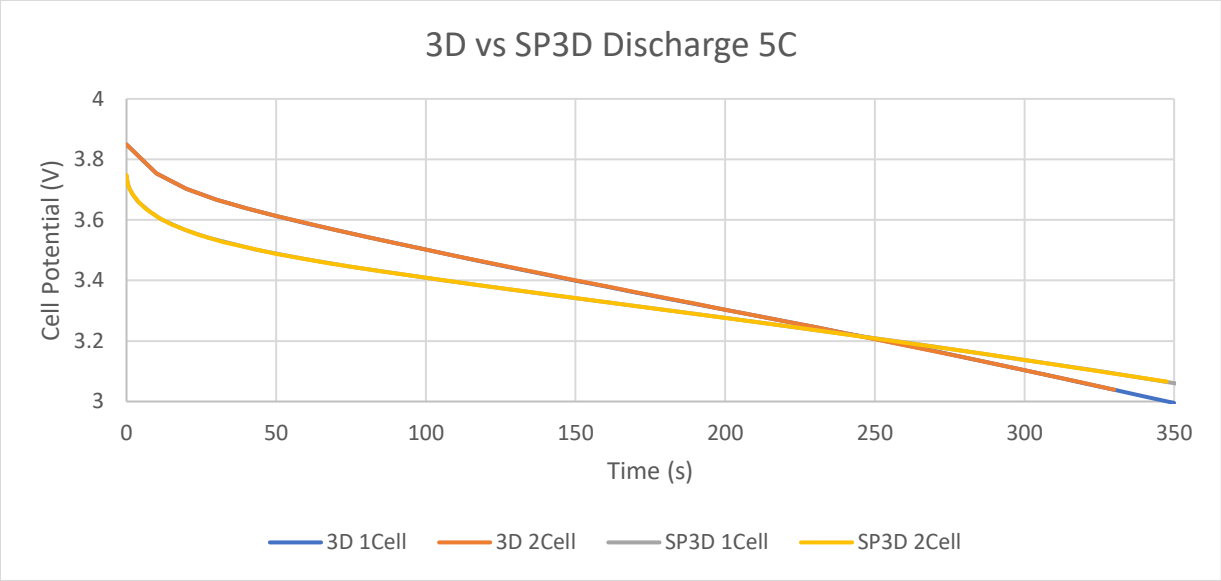

Figure 14: 3D vs SP3D 2Cell 5C Discharge

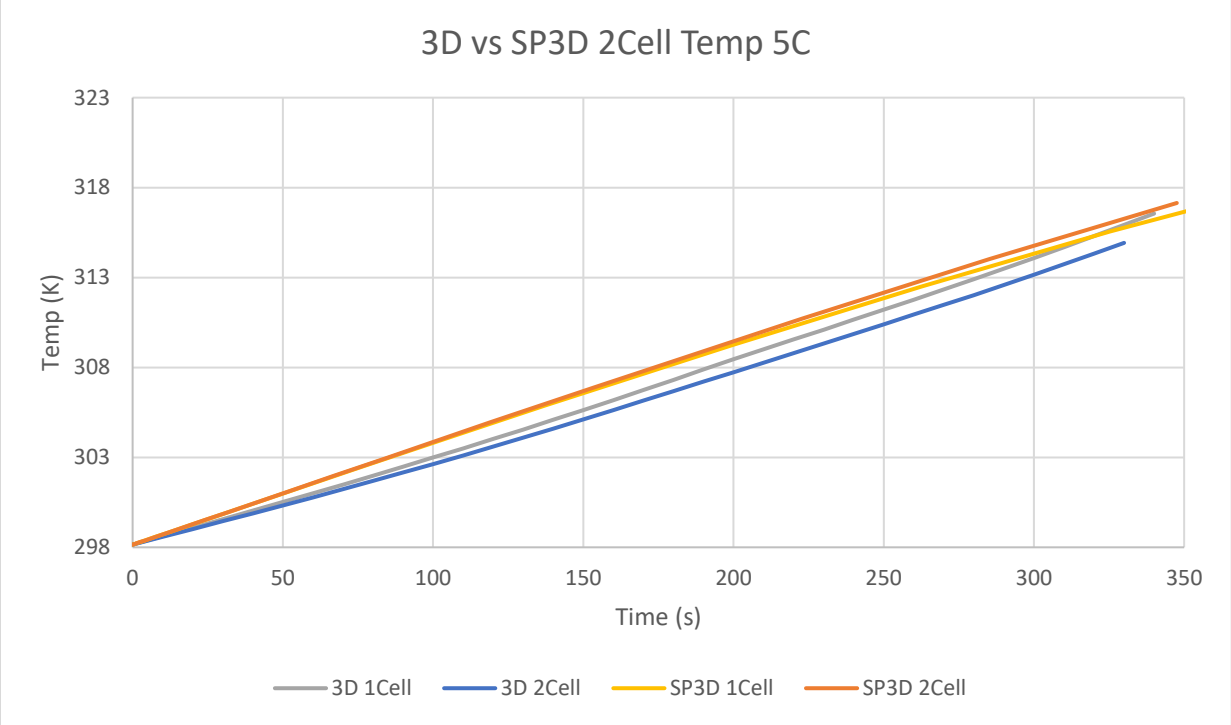

Figure 15: 3D vs SP3D 2Cell 5C Cell Temp

The differences in heat generation were not that profound due to the small cell size. While the SP3D model was successfully tested at up to 15 cells, the 3D model could not successfully compute with such a large pack size. With a more powerful computer and more time, this 3D model can be sized up to test larger models.

The results followed the general trend that was expected. With one exception, the pack models all saw an increase in cell temperature over the single cell models at the same C rate. This change was minor

because due to only sharing one heated surface contact for the pack. However, the 5C 3D discharge was lower than its single cell counterpart and ended discharge early than its specified stop condition at 3V (circled in figure 24). There is no electrochemical reason this should happen, so it indicates an issue with the program. Considering that 11/12 cases follow the expected pattern, I do not believe this issue with 5C 3D invalidates the rest of the results. Further analysis will be conducted on this topic, but the results indicate a technical error.

Lastly, the SP3D model seems to be more affected by pack heat transfer. I believe this is because of the inclusion of the current collectors on the 3D model. By adding the collectors to the positive and negative sides of the battery (composed of aluminum and copper respectfully), the thermal conductivity at these boundaries are altered. There is no way to implement these collectors to the SP3D model because the 3D version does not have specified anode and cathode locations and it only has a total cell heat generation rather than a cathode or anode specific heat generation.

Conclusion

Final analysis of the results at multiple discharge rates and two different pack sizes indicates very strong similarities between the two modeling methods. By comparing the new single particle model with coupled 3D heat generation to the established 3D model with heat generation, the results can be validated. The primary accomplishment of this research project lies in the speed of computation time. The SP3D model can reach these same results in a fraction of the time. While the 3D model can take up to 2 hours to simulate a single cell discharge at 1C, the SP3D model can do the same in 90 seconds. Therefore, a battery model that is both accurate and highly efficient has been successfully created. This low computation time allows the new model to be used in a variety of new scenarios, including further temperature related research and application to battery management systems.

Acknowledgments

I am incredibly grateful for the guidance and support from my advisors Dr. Jonghyun Park and Dr. Robert Landers. The many meetings we have shared has made a huge impact not just on this project, but also my capabilities as a student and engineer.

I would also like to offer my sincere thanks to PhD student Yaqi Zhu and engineer Matthew Hoeppner. Their advice and insight was vital in keeping me directed along the proper path throughout this process.

References

1. Park, J., Seo, J. H., Plett, G., Lu, W., & Sastry, A. M. (2011a). Numerical Simulation of the Effect of the Dissolution of LiMn[sub 2]O[sub 4] Particles on Li-Ion Battery Performance. *Electrochemical and Solid-State Letters*, *14*(2), A14. https://doi.org/10.1149/1.3516619
2. Guo, M., Sikha, G., & White, R. E. (2011b). Single-Particle Model for a Lithium-Ion Cell: Thermal Behavior. *Journal of The Electrochemical Society*, *158*(2), A122. https://doi.org/10.1149/1.3521314
3. Li, J., Landers, R. G., Lofti, N., & Park, J. (2017). A Single Particle Model for Lithium-Ion Batteries with Electrolyte and Stress-Enhanced Diffusion Physics. *Journal of the Electrochemical Society*, *164*(4), 1–3. https://doi.org/10.1149/2.1541704jes
4. Xu, B., Oudalov, A., Ulbig, A., Andersson, G., & Kirschen, D. S. (2018). Modeling of Lithium-Ion Battery Degradation for Cell Life Assessment. *IEEE Transactions on Smart Grid*, *9*(2), 1131–1140. https://doi.org/10.1109/tsg.2016.2578950
5. Cathode Chemistries and Electrode Parameters Affecting the Fast Charging Performance of Li-Ion Batteries. (2020). *JOURNAL OF ELECTROCHEMICAL ENERGY CONVERSION AND STORAGE, 17(2)*, 1–14. https://doi.org/10.1115/1.4045567
6. Ghalkhani, M., Bahiraei, F., Nazri, G.-A., & Saif, M. (2017). Electrochemical–Thermal Model of Pouch-type Lithium-ion Batteries. *Electrochimica Acta*, *247*, 569–587. https://doi.org/10.1016/j.electacta.2017.06.164

Comsol Parameters for SP3D

i_1C	15[A/m^2]	15 A/m²	1C Charge current
Ds_neg	3.9e-14[m^2/s]	3.9E-14 m²/s	Solid phase Li-diffusivity Negative
Ds_pos	1e-13[m^2/s]	1E-13 m²/s	Solid phase Li-diffusivity Positive
rp_neg	12.5e-6[m]	1.25E-5 m	Particle radius Negative
rp_pos	8e-6[m]	8E-6 m	Particle radius Positive
epss_pos	1-epsl_pos-0.259	0.297	Solid phase vol-fraction Positive
epsl_pos	0.444	0.444	Electrolyte phase vol-fraction Positive
cl_0	2000[mol/m^3]	2000 mol/m³	Initial electrolyte salt concentration
epss_neg	1-epsl_neg-0.172	0.471	Solid phase vol-fraction Negative
epsl_neg	0.357	0.357	Electrolyte phase vol-fraction Negative
csmax_neg	26390[mol/m^3]	26390 mol/m³	Max solid phase concentration Negative
csmax_pos	22860[mol/m^3]	22860 mol/m³	Max solid phase concentration Positive
cs0_neg	14870[mol/m^3]	14870 mol/m³	Initial solid phase concentration neg
cs0_pos	3900[mol/m^3]	3900 mol/m³	Initial solid phase concentration pos
k_neg	2e-10*1e4[m/s]	2E-6 m/s	Reaction rate coefficient Negative
k_pos	2e-10*1e4[m/s]	2E-6 m/s	Reaction rate coefficient Positive
L_neg	100e-6[m]	1E-4 m	100e-6Length of negative electrode
L_sep	52e-6[m]	5.2E-5 m	Length of separator
L_pos	183e-6 [m]	1.83E-4 m	183e-6 2.33E-4Length of positive electrode
i_app	a*i_1C	15 A/m²	Charge current for parametric study of lumped model
R_solution	.008[ohm*m^2]	0.008 Ω·m²	Solution phase resistance in the cell
a	1	1	Multiplicative factor for the parametric study
T_ref	298.15[K]	298.15 K	Temperature reference
cell.width	sqrt(Acell)	0.04899 m	
cell.depth	L_neg+L_sep+L_pos	3.35E-4 m	
cell.height	sqrt(Acell)	0.04899 m	
Eadp	29[kJ/mol]	29000 J/mol	activation energy for solid phase diffusion coefficient of pos electrode
Eadn	35[kJ/mol]	35000 J/mol	activation energy for solid phase diffusion coefficient of neg electrode
Earn	20[kJ/mol]	20000 J/mol	activation energy for reaction rate constant of anode
Earp	58[kJ/mol]	58000 J/mol	activation energy for reaction rate constant of cathode
R	8.3145[J/(mol*K)]	8.3145 J/(mol·K)	Ideal gas constant
BatCellDense	2007.7[kg/m^3]	2007.7 kg/m³	Battery density
BatCellCp	837.4[J/(kg*K)]	837.4 J/(kg·K)	Battery Heat capacity at constant pressure
BatCellK	32.2 [W*m^-1*K^-1]	32.2 W/(m·K)	Battery Thermal Conductivity
Sp	3*(epss_pos)/rp_pos	1.1138E5 1/m	Total electroactive area of cathode
Sn	3*(epss_neg)/rp_neg	1.1304E5 1/m	
Acell	24e-4[m^2]	0.0024 m²	Cell cross section area
HtTrnsCo	.1[W/(m^2*K)]	0.1 W/(m²·K)	

Comsol Parameters for 3D Model

D1_pos	1e-13[m^2/s]	1E-13 m²/s	Solid phase Li-diffusivity Positive
rp_pos	8.0E-6[m]	8E-6 m	Radius pos particles
c1max_pos	22860[mol/m^3]	22860 mol/m³	Max solid phase concentration Positive
soc0_pos	3900[mol/m^3]/c1max_pos	0.1706	Initial Positive State of Charge
c0_pos	c1max_pos*soc0_pos[mol/m^3]	3900 mol²/m⁶	Initial solid phase conc Positove
Sa_pos	3*(eps1_pos)/rp_pos	1.1138E5 1/m	Specific interfacial surface area
brug	1.5	1.5	Bruggeman coefficient
Rg	8.314[J/(mol*K)]	8.314 J/(mol·K)	Gas constant
Far	96487[C/mol]	96487 C/mol	Faraday's constant
t_plus	0.363	0.363	Cationic transport number
D2	7.5e-11[m^2/s]	7.5E-11 m²/s	Salt diffusivity in Electrolyte
K1_pos	3.8[S/m]	3.8 S/m	Solid phase conductivity Positive
K1_neg	100[S/m]	100 S/m	
c20	2000[mol/m^3]	2000 mol/m³	Initial electrolyte salt concentration
dlnfdlnc	0	0	Activity factor concentration variation
k_pos	2e-10*1e4[m/s]	2E-6 m/s	Reaction rate coefficient Positive
aA_neg	0.5	0.5	
aA_pos	0.5	0.5	Reaction rate coefficient Positive
aC_pos	0.5	0.5	Reaction rate coefficient Positive
aC_neg	0.5	0.5	Reaction rate coefficient Negative
T_	273.15+25	298.15	
omega	9.2305e-7*0+9.6745e-7*0+7.35e-7	7.35E-7	
a	omega/(Rg*T)*0	0 s²·K·mol/(kg·m²)	
eps2_sep	1	1	
eps1_pos	0.297	0.297	Solid phase vol-fraction Positive
eps2_pos	0.444	0.444	Electrolyte phase vol-fraction Positive
eps1_neg	0.471	0.471	Solid phase vol-fraction Negative
eps2_neg	0.357	0.357	Electrolyte phase vol-fraction Negative
L_sep	5.2E-5[m]	5.2E-5 m	

L_pos_base	183e-6[m]	1.83E-4 m		
L_neg	100E-6[m]	1E-4 m		
p	8.37386994	8.3739		
Q	130	130		
wd	(1e-2)/10	0.001		
Adigit	(1e-2)*wd*number	5E-5		
number	5	5		
Acell	24e-4[m^2]	0.0024 m²	24e-4	1.4e-5
i_1C	15[A/m^2]	15 A/m²		
L_pos_base2	0	0		
CRate	1	1		
D1_neg	3.9e-14[m^2/s]	3.9E-14 m²/s		
rp_neg	1.25E-5[m]	1.25E-5 m		
c1max_neg	26390[mol/m^3]	26390 mol/m³		
soc0_neg	(14870[mol/m^3])/c1max_neg	0.56347		
c0_neg	c1max_neg*soc0_neg[mol/m^3]	14870 mol²/m⁶		
Sa_neg	3*(eps1_neg)/rp_neg	1.1304E5 1/m		
k_neg	2e-10*1e4[m/s]	2E-6 m/s		
phi1_0	Eref_pos(c0_pos/c1max_pos)-Eref_neg(c0_neg/c1max_neg)	4.2171		
phi2_0	0	0		